International Journal of Scientific Engineering and Research (IJSER)
ISSN (Online): 2347-3878
Impact Factor (2020): 6.733

# Insulator Iron Cap Corrosion Detection Based on Deep Learning

**Kaicheng Guo[1], Yaxin Yang[2]**

[1]North China Electric Power University, School of Control and Computer, Beinong Road, 2, China
*cather0915[at]163.com*

[1]North China Electric Power University, School of Control and Computer, Beinong Road, 2, China
*yyx961218[at]163.com*

**Abstract:** ***Insulators are mainly used for electrical insulation and mechanical support in power transmission systems. Because insulators are exposed to the environment and affected by leakage current, pollution and moisture, the iron cap of insulators will corrode, leading to pollution flashover accidents. Therefore, this paper proposes a deep learning based method for detecting iron cap corrosion of insulators in transmission and distribution lines. In this paper, Tensor Flow framework and Faster R-CNN algorithm are used to complete the identification task of four kinds of iron cap corrosion states of glass insulators and porcelain insulators. In this paper, the data set is augmented, the generated number and aspect ratio of anchors in RPN network are improved, and three feature extraction networks are used for comparison. The test results show that the model can effectively detect the corrosion of insulator iron caps in the line, with mAP of 83.50% and an average detection time of 0.186s per image.***

**Keywords:** Insulator, Insulator corrosion, Faster R-CNN, Deep learning

## 1. Introduction

In recent years, with the development of the power system, the scale of the power grid is also gradually expanding. The transmission and distribution lines in the electric power system bears the responsibility of electric energy transmission. The normal operation of the transmission and distribution lines directly affects the stable development of the national economy. Insulator is one of the important external insulation equipment in transmission and distribution lines. The main function of insulator is insulation and support. Therefore, regular inspection of the state of insulator is of great significance to the normal operation of power system [1]. At present, glass insulators and porcelain insulators, which are widely used in power lines, are composed of insulating parts and metal fittings. Due to the metallic characteristics of insulator fittings, insulators may suffer from electrolytic corrosion and galvanic corrosion due to leakage current in daily operation, and may also cause insulator corrosion defects due to the action of industrial gases, acid rain and other corrosive media in the air [2]. The iron cap corrosion of insulators will affect the electrical and mechanical properties of insulators, specifically manifested as the decrease of mechanical strength of insulators and the easy occurrence of flashover accident [3]. According to calculation, the loss caused by corrosion of porcelain insulators accounts for about 2-5% of the GNP of each country [4].

At present, the main detection method of insulators corrosion is manual inspection. In addition, there are other studies, such as on-line monitoring of leakage circuit by adding current loop to insulators. Complex outdoor environment will bring great challenges to manual inspection, such as low efficiency, large consumption of manpower and material resources, and low security of inspection personnel [5]. The installation of leakage current detection device for insulators can effectively judge the insulator's insulation state, but the implementation of full coverage of online current detection device will cost a lot of manpower and material resources.

In recent years, the electric power industry began to use unmanned aerial vehicles (UAVs) to assist manual patrol inspection. The images captured by UAVs are transmitted to the staff on the ground or in the command center for fault judgment [6]. The traditional UAV-based recognition algorithm mainly uses the shape and texture features of the target to detect. Shang et al. [7] used the maximum inter-class variance method to segment the insulators, then extracted the insulator invariant moment eigenvalue, and finally used the Adaboost classifier to locate the insulator position. Ju Zeli et al. proposed an improved semi-interactive segmentation algorithm, which extracted the foreground of a group of similar scenes quickly and accurately, and detected the corrosion on the segmented images according to the corrosion characteristics [8]. Compared with the traditional rod-climbing inspection and helicopter inspection, the inspection method based on UAV saves a lot of manpower, but it still has some shortcomings such as unstable detection results and inaccurate fault identification. UAV images taken during the process of inspection usually has a large amount of data, the low proportion of suspected fault place image, these features for the traditional uav detection is very unfriendly, and in the power equipment deployment environment complex, equipment category is various, the traditional target identification method for promotion and application, so using intelligent image recognition method has great prospects.

In this paper, TensorFlow framework and Faster R-CNN algorithm are used to identify insulators in transmission and distribution lines, and to classify the corrosion of insulators. Faster R-CNN, as a two-stage detection algorithm, has higher accuracy and Faster detection time compared with other one-stage detection algorithms. The rest of this paper is as follows. The methodology used in this paper is described in Section 2. In Section 3, data set, training and testing models

are introduced. In Section 4, the test results of the model are presented and analyzed in this paper. Finally, the work of this paper is summarized in Section 5.

## 2. Methodology

### 2.1 Experiment environment

Table-1 shows the software and hardware configurations used in this article. All experiments in this paper are based on this environment.

**Table 1:** Experiment environment

| Software and hardware platform | Specifications |
|---|---|
| Operating system | Windows |
| Deep learning framework | Tensorflow |
| Central processing unit | Intel Xeon Gold 5120T |
| Graphics processing unit | GeForce RTX 2080Ti |

### 2.2 Model Framework

In this paper, TensorFlow framework and Faster-RCNN algorithm are used to identify and classify iron cap corrosion defects of insulators in transmission and distribution lines. The detection process of the Faster-RCNN algorithm is shown in Fig. 1. First, the input image is adjusted to the appropriate size, and then the feature is extracted using the feature extraction network. In this paper, three Feature extraction networks, namely VGG-16, ResNet-50 and ResNet-101, were compared and used to extract features to obtain Feature maps, which were shared for subsequent candidate region generation networks and full connection layers. The RPN network maps a large number of anchor frames on the original image, determines whether the anchor frames belong to the foreground or the background, and then obtains the candidate regions through regression correction. In the Roipooling stage, the candidate areas obtained by RPN are mapped to the Feature map generated by the Feature extraction network, and then the candidate boxes of different sizes are pooled into Feature vectors of equal length, which are used as the input of the subsequent full connection layer. Finally, the object types are finely judged in the full connection layer and the frame is finally adjusted.

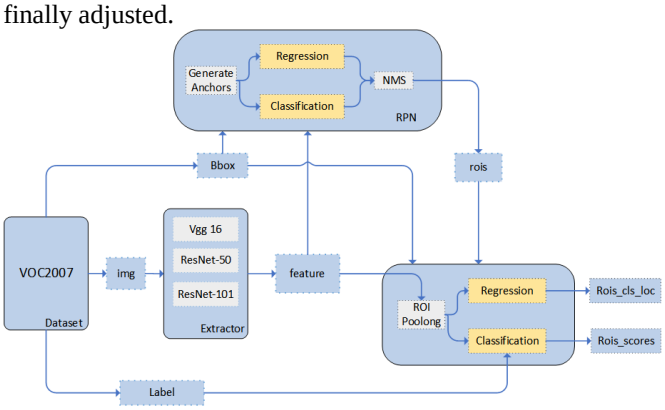


**Figure 1:** Model framework

### 2.3 Feature extraction network

In this paper, three feature extraction networks are compared and used, namely VGG-16, ResNet-50 and ResNet-101. The following number represents the number of layers of the network. Generally speaking, the deeper the network is, the better the performance will be. However, as the number of network layers increases, the correlation between gradients will get worse and worse during the back propagation and finally approach white noise. In this case, the update of gradient may be doing random disturbance [12]. The emergence of ResNet solves the problem of deep network degradation. The core of ResNet is a (bottleneck design) residual block, as shown in Fig. 2.

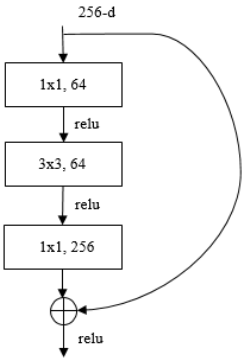


**Figure 2:** ResNet block

The residuals block uses a "Shortcut Connection" connection that makes reference(X) to the input at each layer to form the residuals function. The use of residual function makes the model easier to optimize. Table-2 and Table-3 show the network structure of VGG-16, ResNet-50 and ResNet-101, respective.

**Table 2:** Vgg-16

| Layer name | Vgg-16 |
|---|---|
| Block1 | $[Conv3-64]\times 2$ |
| | maxpool |
| Block2 | $[Conv3-128]\times 2$ |
| | maxpool |
| Block3 | $[Conv3-256]\times 3$ |
| | maxpool |
| Block4 | $[Conv3-512]\times 3$ |
| | maxpool |
| Block5 | $[Conv3-512]\times 3$ |
| | maxpool |
| FC-4096 | |
| FC-4096 | |
| FC-4096 | |

**Table 3:** ResNet-50, ResNet-101

| Layer name | ResNet-50 | ResNet-101 |
|---|---|---|
| Conv1 | 7×7, 64, stride 2 | |
| | 3×3 max pool,stride 2 | |
| Conv2_x | $\begin{bmatrix}1\times1,64\\3\times3,64\\1\times1,256\end{bmatrix}\times3$ | $\begin{bmatrix}1\times1,64\\3\times3,64\\1\times1,256\end{bmatrix}\times3$ |
| Conv3_x | $\begin{bmatrix}1\times1,128\\3\times3,128\\1\times1,512\end{bmatrix}\times4$ | $\begin{bmatrix}1\times1,128\\3\times3,128\\1\times1,512\end{bmatrix}\times4$ |

| | | |
|---|---|---|
| Conv4_x | $\begin{bmatrix}1\times1,256\\3\times3,256\\1\times1,1024\end{bmatrix}\times6$ | $\begin{bmatrix}1\times1,256\\3\times3,256\\1\times1,1024\end{bmatrix}\times23$ |
| Conv5_x | $\begin{bmatrix}1\times1,512\\3\times3,512\\1\times1,2048\end{bmatrix}\times3$ | $\begin{bmatrix}1\times1,512\\3\times3,512\\1\times1,2048\end{bmatrix}\times3$ |

### 2.4 RPN network

Compared with its predecessor algorithm, the biggest change of Faster R-CNN is that the candidate region generation network is proposed, so that the candidate region generation and subsequent classification regression are completed by the neural network, and the weight can be shared at the same time, which greatly improves the training and detection speed of the algorithm. The structure of RPN is shown in Fig.3.

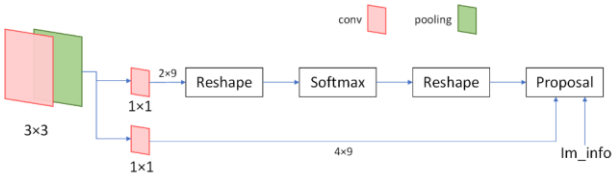


**Figure 3:** The structure of RPN

The RPN network is divided into two branches. After the 3x3 convolution of the feature figure, the foreground (background) classification was obtained by the softmax classification of Anchor, and the bounding box regression offset of Anchor was calculated by the secondary line 2. The final proposal layer is responsible for synthesizing the position anchor and the corresponding bounding box offsets and eliminating the small ones that exceed the boundary, so as to complete the function of target detection.

### 2.5 Loss function

The loss function of Faster R-CNN is divided into the loss of RPN and the loss of Roipooling, both of which include classification loss and regression loss. Equation (1) is the sum of losses. The preceding items are classified losses and the following items are regression losses.

$$L(\{p_i\},\{t_i\}) = \frac{1}{N_{cls}}\sum_{i=1}^{N} L_{cls}(p_i, p_i^*) + \lambda \frac{1}{N_{reg}}\sum_{i=1}^{N} p_i^* L_{reg}(t_i, t_i^*) \quad (1)$$

Where $N_{cls}$ is the size of the mini batch 256, $N_{reg}$ is the size of the feature map, and $\lambda$ is the weight balance parameter.

The classification loss of RPN is the binary cross-entropy loss of foreground (target) and background, while the classification loss of Roihead is the quad-classification cross-entropy loss of which insulator is determined. Equation (2) is the binary cross-entropy loss, which is the same with the quad-classification cross-entropy loss. Where $i$ is the serial number of the anchor, and $p_i$ is the probability that the anchor predicts to be a target. When there is a target object in the anchor, $p_i^*$=1; otherwise, it is 0.

$$L_{cls}(p_i, p_i^*) = -log\left[p_i^* p_i + (1-p_i^*)(1-p_i)\right] \quad (2)$$

The position regression of the target box is initially determined by RPN network, and then fine calibration is performed by ROIpooling. The regression loss is shown in Equations (3), (4) and (5) below. Where $t_i$ represents the predicted offset of the anchor, and $t_i^*$ is the actual offset of the anchor relative to the ground ture. $R(x)$ is the smoothL1 function.

$$\begin{aligned} &t_x = (x - x_a)/w_a, t_y = (y - y_a)/h_a, \\ &t_w = \log(w/w_a), t_h = \log(h/h_a), \\ &t_x^* = (x^* - x_a)/w_a, t_y^* = (y^* - y_a)/h_a, \\ &t_w^* = \log(w^*/w_a), t_h^* = \log(h^*/h_a), \end{aligned} \quad (3)$$

$$L_{reg}(t_i, t_i^*) = R(t_i - t_i^*) = R(x) \quad (4)$$

$$R(x) = \begin{cases} 0.5x^2 & |x| < 1 \\ |x| - 0.5 & otherwise \end{cases} \quad (5)$$

## 3. Model training and testing

This chapter mainly introduces the pre-processing of data and the production of data sets. Meanwhile, the details of model training and testing will also be described in this chapter.

### 3.1 Date set

Since there is no public data set of transmission and distribution network at present, this paper selects 1,500 images from UAV transport inspection images of transmission and distribution lines in a province of China. Based on the mechanical and electrical properties of insulators, the corrosion types of insulators mainly detected in this paper fall into four categories: intact insulators, only iron cap corrosion, only corrosion product channels, and insulators with corrosion product channel and iron cap corrosion. Each image contains one or more insulators. After statistics, the number of all kinds of insulators in the 1500 images is given in the Table-4.

**Tabel 4:** Data set category distribution

| Insulator corrosion type | Label | Number |
|---|---|---|
| Intact corrosion | insulator | 1777 |
| Only iron cap corrosion | insulator_corrosion1 | 998 |
| Only corrosion product channel | insulator_corrosion2 | 595 |
| Corrosion product channel and iron cap corrosion | insulator_corrosion3 | 817 |
| Total | | 4187 |

In order to reduce the computational burden of the model, this paper scales the screened images to 1024*768 pixels in the original size in advance, and then uses the Labelimg software to frame select four types of insulators in the image and generate four types of XML files with object labels and coordinates. The dataset is formatted in Pascal Voc2007 and consists of a JPEGImages folder for images, a Annotations folder for object labels and coordinate information, and an ImageSets folder for splitting training sets, validation sets, and test sets. The data set is distributed in a 6:2:2 ratio of training set, verification set and test set, that is, 900 pieces of training set, 300 pieces of verification set and 300 pieces of test set. In order to obtain better training effect, this paper uses the data augment method of mirror inversion and rotation of 30° for the training set and the verification set to augment the

data. The number of each data set after augment is: 3600 training sets, 1200 verification sets and 300 test sets.

### 3.2 Feature extraction network

In this paper, the performance of the three feature extraction networks is investigated by using the control variable method, that is, except replacing the feature extraction network, the other parameters remain the same. After the network training based on the three features extraction, the model was tested, and the obtained PR curves were shown in Fig.4. The AP of each category was the area enclosed by its PR curves.

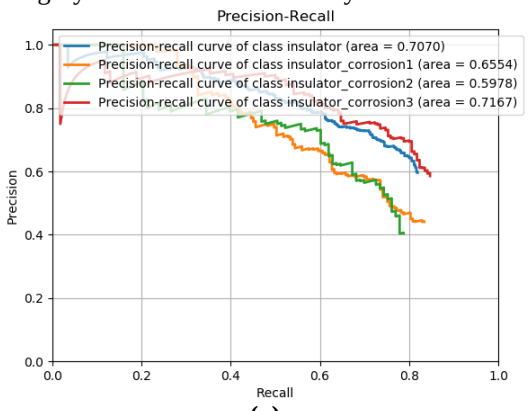


**(a)**

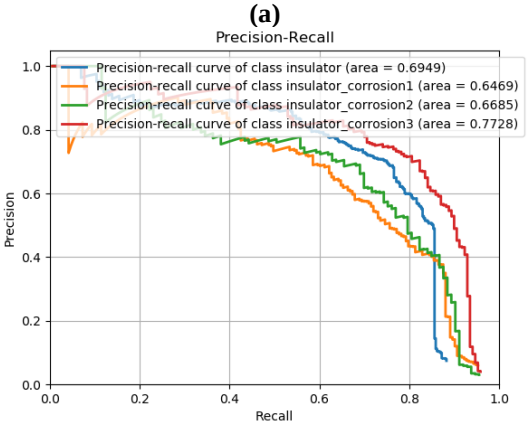


**(b)**

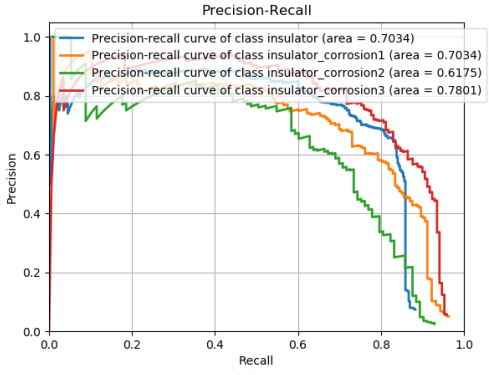


**(c)**

**Figure 4:** PR curve.(a)Vgg-16,(b)ResNet-50,(c)ResNet-101.

As can be seen from the figure, the average accuracy of VGG-16, ResNet-50 and ResNet-101 has been gradually improved, and the recall rate of ResNet series has been greatly improved compared with VGG-16. It can be concluded that ResNet-101 has the best performance among the three networks. Therefore, the follow-up work of this paper is based on ResNet-101.

### 3.3 RPN

During the production of the data set, it was observed that most of the high-voltage insulators were thin and long, and most of them were in the V-shaped state, vertical state or horizontal state. Moreover, it was also found in the test results of the preliminary training model that the model had a certain probability of missed detection for the slender insulators in the vertical state. Combining the above two aspects, this paper decided to add a new type of anchor with the aspect ratio of 1:3 and 3:1 in the generation of anchor, on the basis of the original aspect ratio of [1:1,1:2,2:1]. That is, 3×5 = 15 anchors (3 types of areas and 5 types of rectangles) are now generated from the original 3×3 = 9 sizes and unequal areas. Fig.5 shows the new anchor generation mechanism with fixed area and varying length and width.

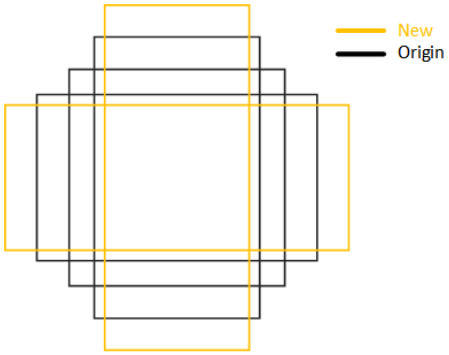


**Figure 5:** New anchor frame generation mechanism

It is also found that the occlusion of insulators side by side in the data set will lead to missed detection of the model. In view of this situation, this paper finds out the pictures which are seriously caused by insulator occlusion in the test results, and carries out IoU calculation on the insulators side by side in the pictures. By calculating the IoU of side-by-side insulators, the NMS threshold of the non-maximum suppression algorithm is adjusted to 0.55 in this paper. The experiment shows that the situation of missed detection has been improved to some extent.

At the same time, this paper also adjusts the number of ROIs in RPN network. The PR diagram of the model after the improvement of Anchor in RPN is shown in Fig.6, and the accuracy of the model has been greatly improved.

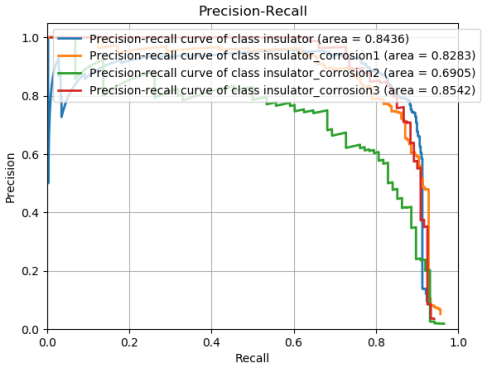


**Figure 6:** PR curve after improving the anchor

### 3.4 Test part

In the test stage, this paper used function packages such as Matplotlibt, PyLab and Sklearn to process the prediction information of the model output, carried out IoU operation on the coordinate box and Ground-true of the prediction information, and the PR graph in this paper was output based on this method. Fig.7 shows the schematic diagram of IoU operation. IoU of two boxes is the intersection of two boxes divided by union.

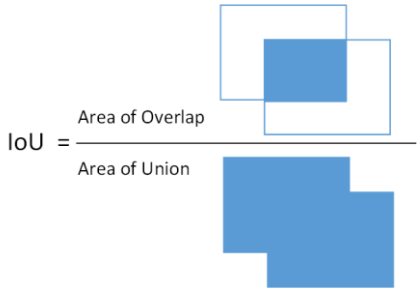


**Figure 7:** IoU calculation method

For the prediction box with Ground-true IoU > 0.5, determine that the prediction box is correct. Then, the accuracy rate and recall rate of each category were counted, PR curve was output, and AP and mAP of each category were calculated.

### 3.5 Model paramaters

After repeated training and adjustment, the parameters of the model are shown in the following Table-5. At this time, the PR diagram of the model test is shown in Fig.8.

**Table 5:** Model parameter

| **Parameter** | **Value** |
|---|---|
| Max iteration | 50000 |
| learning rate | 0.001 |
| weight decay | 0.0001 |
| **Batch size** | **Value** |
| Images to use per minibatch | 1 |
| number of regions of interest | 128 |

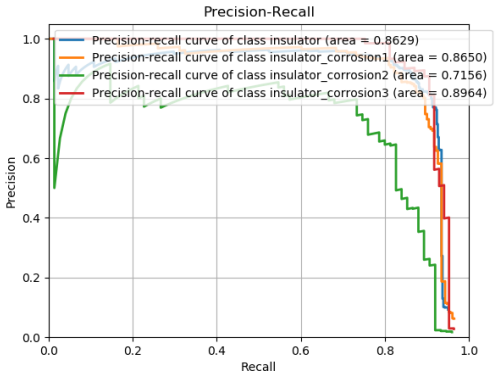


**Figure 8:** PR curve after adjusting the training parameters

## 4. Result and analysis

After improving the anchor and adjusting the training parameters of the model, the accuracy rate and detection time of the model are shown in Table-6.

**Table 6:** AP and detection time

| **Label** | **AP (%)** |
|---|---|
| insulator | 86.29 |
| insulator_corrosion1 | 86.50 |
| insulator_corrosion2 | 71.56 |
| insulator_corrosion3 | 89.64 |
| **mAP** | **83.50** |
| **Detection time** | **0.186s** |

The intact insulators and the first and third type of corrosion have higher accuracy, while the detection accuracy of the second type of corrosion is relatively low. The reasons for the low accuracy of the second type of corrosion are as follows:

(1) The characteristics of the second type of corrosion are more difficult to capture than those of the other three types, and they are consistent with intact insulators except for corrosion product channels, with a high degree of similarity. Therefore, it is easy for the model to determine the second type of corrosion as the intact insulator, resulting in the missed detection of the second type of corrosion insulator. This inference can be verified from the PR figure. Compared with the other three types of corrosion, the green line representing the second type of corrosion has the lowest Recall value.

(2) Although the ratio requirement of balance between classes of training data is met during the production of data sets (the ratio between classes should not exceed 1:4), the number of insulators corrode in the second type is the least, which provides less training information for the training model compared with the other three types. Although this situation can be improved to some extent after data enhancement, supplementing this kind of data set is still the most effective means to improve this kind of accuracy.

Since there is currently no literature on using deep learning to detect insulator corrosion in transmission and distribution lines, this paper makes a horizontal comparison with other models using deep learning to identify insulators and their defects. The comparison results are shown in Table-7.

**Table 7:** Comparison experiment

| Method | Detect defect type (Except for normal insulator) | mAP (%) | Detection time (second/ piece) |
|---|---|---|---|
| Faster R-CNN by Liao et al.[9] | Missing cap and lighting strike | 89.20 | 0.517 |
| YOLOv3 by Adou et al.[10] | Missing cap | 83.52 | Not mentioned |
| Multi-Task Learning by Prates et al.[11] | Broken insulator | 85.50 | Not mentioned |
| **Faster R-CNN in this paper** | Insulators with four types of corrosion | 83.50 | 0.186 |

Compared with the other three classification tasks in Table 6, the average accuracy of this paper is slightly lower. The reasons why the average accuracy of this paper is lower than that of the three literatures are as follows:

(1) Except for the second type of corrosion insulators, the detection accuracy of intact insulators and the first and third type of corrosion insulators are all higher than that of two of the three papers. The significant decrease in

the average accuracy of this paper comes from the poor performance of detecting the second type of corrosion.

(2) The problems solved in this paper are somewhat more difficult than those in the comparative literature. In the detection tasks in the three literatures, insulator damage and missing would intuitively show the missing insulator contour in the pictures. In the feature extraction stage, the change of object contour is easier to be captured by the feature extraction network. In this paper, the four types of insulators detected are all complete in contour, with only the texture differences on the insulator iron cap and the surface area.

In this article, the test set was 20% of the original screened images and did not participate in data augment. The recognition effect of the model is to mark the insulator in the image for each input image, give the corrosion type of the insulator iron cap and give the confidence score. The detection effect is shown in Fig.9. In Fig.9(a), two intact insulators are detected. In Fig.9(b), two insulator_corrosion1 are detected. In Fig.-9(c), four insulator_corrosion2 and one insulator_corrosion1 are detected. In Fig.9(d), two insulator_corrosion3 are detected.


(a)

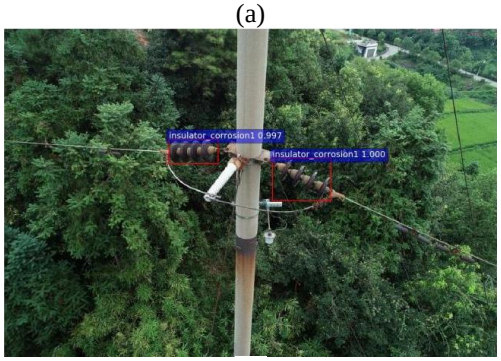


(b)

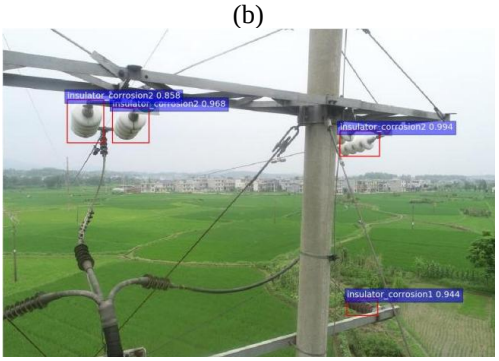


(c)


(d)

**Figure 9:** The detected results. (a) Two intact insulators, (b) Two insulator_corrosion1, (c) Four insulator_corrosion2 and one insulator_corrosion1, (d) Two insulator_corrosion3

## 5. Conclusion

This paper presents an intelligent detection method for the type of iron cap corrosion of insulators in overhead transmission and distribution lines. The four iron cap corrosion states of insulators, including no corrosion, only iron cap corrosion, only corrosion product channel, and insulators with corrosion product channel and iron cap corrosion, were identified and detected by using TensorFlow framework and Faster R-CNN convolutional neural network. The performance of the three feature extraction networks in this task was compared. According to their PR curves, it was concluded that ResNet-101 had the best detection effect, followed by ResNet-50 and VGG-16. In the process of RPN, anchors with length-to-width ratios of 1:3 and 3:1 were added to preliminarily fit the shape of the insulator. The experimental results showed that the accuracy and recall rate of the model were improved to a certain extent. In this paper, the prediction information of the model is verified by calculating the overlap degree of the predicted object box and ground-true to replace manual result statistics. The test results' mAP is 83.50%, and the average detection time of a single image is 0.186s. This method can effectively detect the corrosion of insulators in transmission and distribution lines and provide safety guarantee for the normal operation of power grid.

## References

[1] Z. Yuan, Y. Tu, R. Li, F. Zhang, B. Gong, and C. Wang, "Review on Characteristics, Heating Sources and Evolutionary Processes of the Operating Composite Insulators with Abnormal Temperature Rise," *CSEE Journal of Power and Energy Systems*, DOI: 10.17775/CSEEJPES.2019.02790.

[2] L. Luo *et al.*, "Research on the electrolytic corrosion problem of porcelain insulator's hardware on UHVDC transmission line," *2014 IEEE Electrical Insulation Conference (EIC)*, 2014, pp. 97-101,doi: 10.1109/EIC.2014.6869355.

[3] L. Luo *et al.*, "Study on mechanical and electrical characteristics of gossans electrochemical corrosion ceramic insulators on DC transmission line," *2013 Annual Report Conference on Electrical Insulation and Dielectric Phenomena*, 2013, pp. 411-414, doi: 10.1109/CEIDP.2013.6748132.

[4] Sanyal, S., Kim, T., Jeon, S., Lee, Y.-J., Yi, J., Choi, I.-H., Son, J.-A., Koo, J.-B. Influence of Corrosion on Electrical and Mechanical Properties of Porcelain Suspension Insulators: An Overview (2020) Transactions on Electrical and Electronic Materials, 21 (6), pp. 543-549.

[5] S. Chen, "Problems Analysis and Countermeasures of Inspecting Electric Power Equipment," *Electric power manufacturing technology and equipment*, vol. 0, no. 5, pp. 130-137, 2015.

[6] H. He, Y. Zhu, and W. Yuan, "Application of small multi-rotor UAV in overhead transmission line inspection," *Jiangxi Electric Power*, vol. 41, no. 8, pp. 32-35, 2017.

[7] J.Shang *et al*.,"Visual-based insulator localization and self-detonation defect detection".Journal of Electronic Measurement and Instrumentation, 2017,31(06):844-849.

[8] Z. Ju *et al*., "Detection of corrosion defects for transmission lines". Electrical engineering technology, 2020(17):77-81.

[9] G. Liao, G. Yang, W. Tong, W. Gao, F. Lv and D. Gao, "Study on Power Line Insulator Defect Detection via Improved Faster Region-Based Convolutional Neural Network," 2019 IEEE 7th International Conference on Computer Science and Network Technology (ICCSNT),2019, pp. 262-266, doi: 10.1109/ICCSNT47585.2019.8962497.

[10] Adou, M.W., Xu, H., Chen, G.Insulator Faults Detection Based on Deep Learning.(2019) Proceedings of the International Conference on Anti-Counterfeiting, Security and Identification, ASID, 2019-October, pp. 173-177. DOI: 10.1109/ICASID.2019.8925094.

[11] Ricardo M. Prates, Ricardo Cruz, André P. Marotta, Rodrigo P. Ramos, Eduardo F. Simas Filho, Jaime S. Cardoso. Insulator visual non-conformity detection in overhead power distribution lines using deep learning.Computers & Electrical Engineering,Volume 78,2019,Pages 343-355,ISSN 0045-7906.

## Author Profile

**Kaicheng Guo** completed his bachelors in Optoelectronic Information Science and Engineering from Nanjing Tech University ,China, in 2015. Now he is a master's student in the School of Control and Computer, North China Electric Power University, China. His areas of interest include Image Processing, Machine learning and Deep learning.

**Yaxin Yang** is a master's student in the School of Control and Computer, North China Electric Power University. Her areas of interest include Image Processing, Video Processing, Software development and Machine learning.